Evaluation of the Internal Pressure Capacity at Leak Failure of PWR Containment Building Considering High Temperature and Pressure at Hydrogen Burning Conditions

Woo-Min Cho[a], Yong-Jin Cho[a], Seong-Kug Ha[a*]
[a]Korea Institute of Nuclear Safety (KINS), 62 Gwahak-ro, Yuseong-gu, Daejeon 34142, Korea
**Corresponding author: skha@kins.re.kr*

Keywords : PWR Containment Building, Hydrogen Burning Conditions, Leak Failure, Internal Pressure Capacity

1. Introduction

The Fukushima nuclear accident increased awareness about the importance of robust design for containment structures. This includes severe accidents in nuclear power plants and scenarios exceeding the design basis due to extreme conditions like natural disasters. Investigating the structural integrity of containment buildings is crucial to protect people, property and prevent environmental contamination, despite a low probability of catastrophic accidents.

South Korea was required to implement an accident management program, including severe accident management, after the Nuclear Safety Act was revised in 2016. Materials such as concrete, rebars, tendons, liners, and others change their physical properties when they come into contact with combustible gases in containment buildings during severe accidents. Hence, a practical evaluation considering the temperature-dependent material properties of these components is necessary.

Considering these factors, creating a finite element model for containment buildings in nuclear power plants is crucial. Quantitative assessment of structural integrity should consider thermal and mechanical responses under high temperature and pressure conditions during severe accidents. Heat transfer and thermal stress analyses were conducted in this study to establish the ultimate pressure capacity of the pressurized water reactor (PWR) containment building under hydrogen burning conditions. A liner strain of 0.3% was used to maintain structural integrity, following the recommendation of ASME Section III, Division 2, subarticle CC-3720 [1].

2. Numerical Modeling of PWR Containment

2.1 Constitutive Models and Material Properties

The Concrete Damaged Plasticity (CDP) model was used to demonstrate the nonlinear and inelastic responses of the PWR containment buildings by simulating the concrete response to stress [2]. Hognestad and Izumo's theoretical models were used to illustrate compression and tension in concrete, as described in Eqs. 1 and 2 [3,4].

$$\sigma_c = \begin{cases} f_c\left[2\left(\frac{\varepsilon}{\varepsilon_0}\right) - \left(\frac{\varepsilon}{\varepsilon_0}\right)^2\right] & \text{for } \varepsilon \le \varepsilon_0 \\ f_c\left(1 - 0.15\frac{\varepsilon - \varepsilon_0}{\varepsilon_{cu} - \varepsilon_0}\right) & \text{for } \varepsilon > \varepsilon_0 \end{cases} \quad (1)$$

$$\sigma_t = \begin{cases} E \times \varepsilon & \text{for } \varepsilon \le \varepsilon_{cr} \\ f_t & \text{for } \varepsilon_{cr} < \varepsilon \le \varepsilon_0 \\ \left(\frac{2\varepsilon_{cr}}{\varepsilon}\right)^{0.4} & \text{for } 2\varepsilon_{\mathrm{cr}} < \varepsilon \end{cases} \quad (2)$$

$$\varepsilon_0 = 1.8(f_c/E) \quad (3)$$

where f and σ denote strength and stress, with subscripts c and t implying compression and tension. The crushing ε_{cu} is set at 0.0038 and ε_0 represents the strain at f_c expressed by Eq. 3. Additionally, ε_{cr} denotes the cracking strain. Table 1 presents the material properties of concrete, including parameters such as density (ρ), elastic modulus (E), Poisson's ratio (ν), dilation angle (ψ), eccentricity (m), the ratio of biaxial to uniaxial compressive strength (β) and invariant ratio (K_c).

Table 1. Material properties of concrete [6]

ρ (ton/mm^3)	E (GPa)	ν	f_c (MPa)
2.5×10^{-9}	26.6	0.18	35
ψ	m	β	K_c
34	0.1	1.16	0.667

An elasto-plastic model with isotropic hardening was used to analyze the behaviors of steel components such as the liner, rebar, and tendon, as shown in Eq. 4 [2]. Table 2 summarizes the material properties of steel components. The value of v is consistently 0.3 for all steel components.

$$f = \sigma_e - \sigma_y = \left(\frac{3}{2}s{:}s\right)^{1/2} - \sigma_y \quad (4)$$

where s represents the deviatoric stress, σ_e denotes the von Mises stress, σ_y is the yield stress.

Table 2. Material properties of steel [6]

Component	ρ (ton/mm^3)	E (GPa)	σ_c (MPa)
Rebar	7.85×10^{-9}	200	460.0
Liner	7.80×10^{-9}	220	453.0
Tendon	7.41×10^{-9}	196	1,297.4

2.2 Details of FE Model

Details of the finite element modeling can be found in Cho et al [6]. The finite element analysis used 3D, 8-node brick elements with reduced integration (C3D8R) for concrete, 4-node quadrilateral shell elements with reduced integration (S4R) for liner plates, and 3D, 2-node elements (T3D2) for rebar in structural analysis [6]. Figure 1 shows the constraint for all degrees of freedom, such as nodes and elements, at the bottom face of the basemat, which is loaded by internal pressure applied perpendicular to the liner.

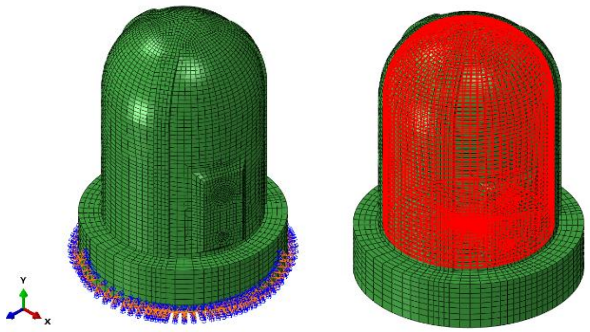

(a) (b)

Fig. 1. Boundary and loading conditions [6]

3. Evaluation of Internal Pressure Capacity at Leak Failure subjected to Hydrogen Burning Conditions

The study utilizes the MELCOR2.2 code to simulate pressure and temperature under hydrogen burning conditions for the PWR design [6]. Under full power operation, long term station-blackout sequences were analyzed without PAR (Passive Auto-Catalytic Recombiner) and operator action [6]. Figure 2 illustrates the temperature and pressure profiles subjected to hydrogen burning conditions.

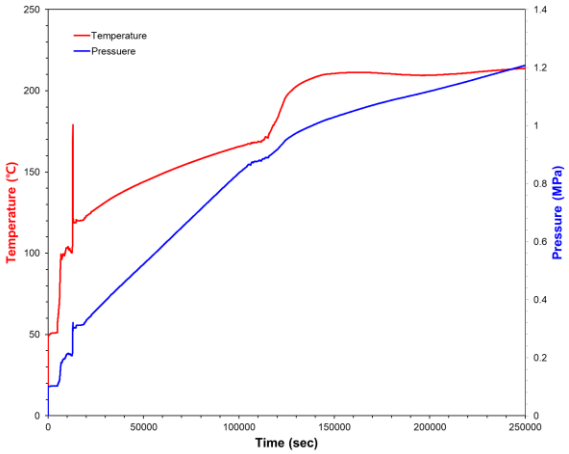

Fig. 2. Temperature and pressure histories subjected to the hydrogen burning conditions [6]

3.1 Mesh Sensitivity Analysis

A mesh sensitivity analysis was carried out to develop the finite element model accurately. The analysis involved using four different element sizes (200 mm, 300 mm, 400 mm, and 500 mm). Figure 3 shows the radial displacement of the liner in accordance with the pressure conditions described in Fig. 2 [6]. The finite element model with a 300 mm element size was selected based on the analysis results indicating convergence for element sizes smaller than 300 mm [6].

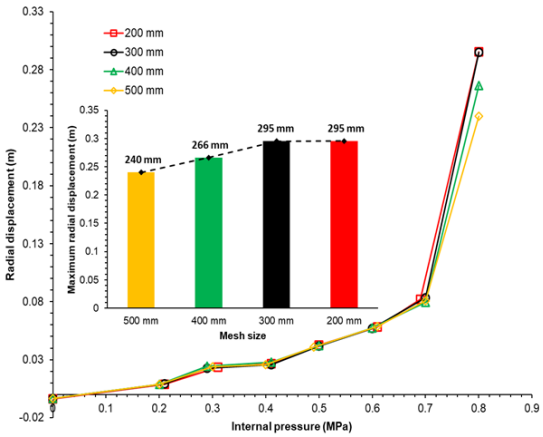

Fig. 3. Mesh sensitivity analysis [6]

3.2 Thermal Behavior under Hydrogen Burning Conditions

The element types used for the heat transfer analysis were changed to linear heat transfer brick (DC3D8) for concrete, 4-node heat transfer quadrilateral shell (DS4) for the liner, and 2-node heat transfer link (DC1D2) for rebar and tendon. The thermal characteristics of each part were considered, as listed in Table 3.

Table 3. Thermal properties for concrete and steel [6]

Component	Conductivity (W/m×℃)	Specific heat (J/kg×℃)	Thermal expansion ($℃^{-1}$)
Concrete	1.4	879	1.0×10^{-5}
Steel	45	470	1.2×10^{-5}

The study analyzed how mechanical properties change with temperature for both concrete and steel, as described by Eqs. 5 to 8 [7].

Concrete strength ratio
$$S_{Rc} = \exp^{-}(T/632)^{1.8} \quad (5)$$

Concrete modulus ratio
$$M_{Rc} = (S_{Rc})^{0.5} \quad (6)$$

Steel yield strength ratio
$$S_{Rs} = \exp^{-}((T-340)/300)^{1.9} \quad (7)$$
$$S_{Rs} = 1.0, T \leq 340℃$$

Steel modulus ratio
$$M_{Rs} = S_{Rs} \quad (8)$$

Figure 4 shows the decrease in strength ratios and modulus ratios of concrete and steel components in response to changes in temperature [7].

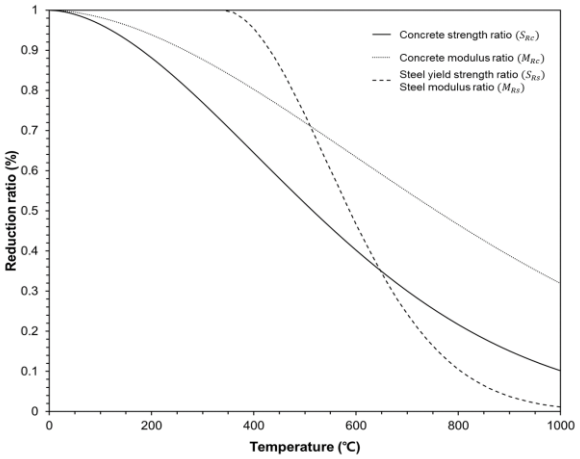

Fig. 4. Reduction ratios of strengths and modulus ratios according to the temperature variations [7]

Thermal boundary conditions were applied to the outer surface of the concrete region of the PWR containment building for heat transfer analysis. The conditions involved free convection with air at a sink temperature of 25 ℃ and a heat convection coefficient of h_conv [6]. The heat conduction coefficient, h_cond, at the basemat with soil was considered at a sink temperature of 25 ℃ [6]. Equations 9 and 10 detailed the changes in heat transfer coefficients based on temperature [6,7].

$$h_{conv} = 1.20(\Delta T)^{1/3}\ W/m^2 \cdot K \quad (9)$$

$$h_{cond} = 0.0181\ W/m^2 \cdot K \quad (10)$$

The temperature data shown in Fig. 4 was used as a boundary condition for the liner nodes in the heat transfer analysis [6]. The heat transfer analysis was conducted using the prescribed thermal properties and boundary conditions [6]. Figure 5 shows the temperature distribution during hydrogen burning, with a peak temperature of 179.1 ℃ [6]. Figure 6 displays the thermal gradient of the concrete in the direction of thickness over time, with d/T representing the depth per thickness.

3.3 Mechanical Behavior under Hydrogen Burning Conditions

A structural analysis was conducted to evaluate the mechanical response of the PWR containment building to temperature and internal pressure loads. Utilizing the *Predefined Field, Temperature option in ABAQUS software, the heat transfer analysis results were applied as a thermal boundary condition [6].

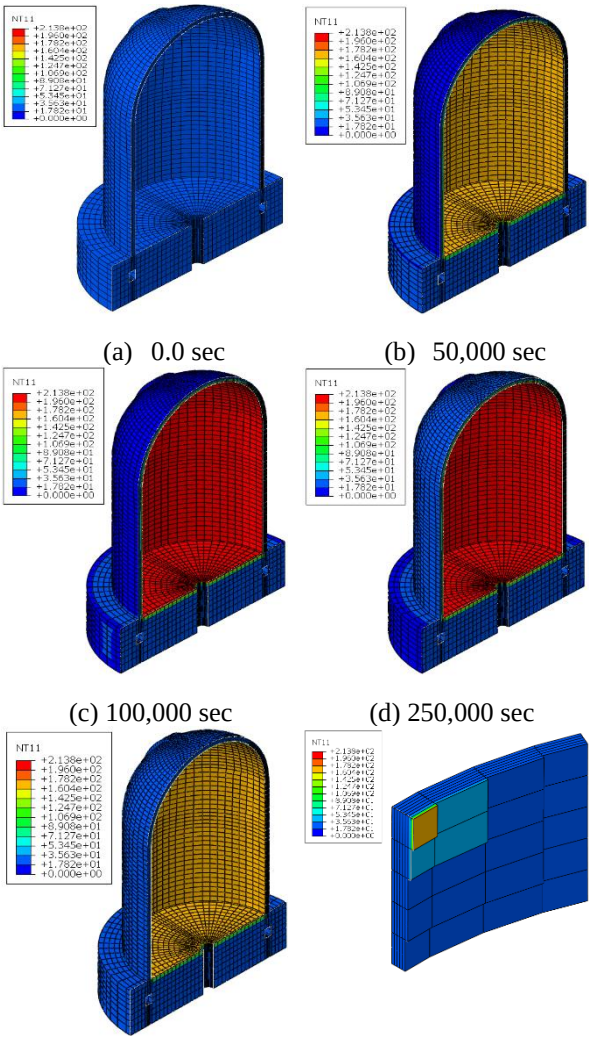

(a) 0.0 sec (b) 50,000 sec

(c) 100,000 sec (d) 250,000 sec

(e) 12,900 sec (peak) (f) 12,900 sec (peak)

Fig. 5. Temperature distribution at the hydrogen burning conditions (unit: ℃) [6]

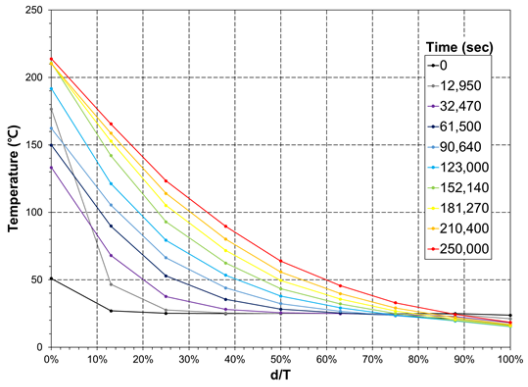

Fig. 6. Thermal gradients of concrete according to depth per thickness [6]

This study investigates leak failure caused by liner tearing, using the failure criteria of 0.3% liner strain

recommended by ASME Section III, Division 2, sub-article CC-3720.

Figure 7(a) and 7(b) show the maximum principal strain distributions of the liner near the equipment hatch (EH) region and the free field (FF) region away from discontinuities, respectively. The liner reached a maximum strain of 1.92% at the left side of the EH after 250,000 seconds. Figure 8 shows the maximum principal strains of the liner at the EH and FFs located on the left and right sides of EH, in comparison to the failure criteria of 0.3 % liner strain [6]. Liner tearing is expected to occur at 0.61 MPa at the EH, and at 0.67 MPa and 0.66 MPa at the left FF and right FF regions, respectively.

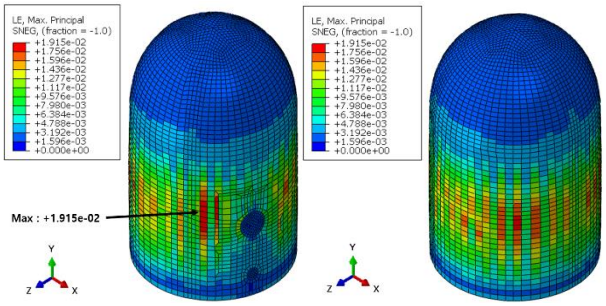

(a) EH region (b) FF region

Fig. 7. Distributions of maximum principal strains of the liner (unit: mm/mm) [6]

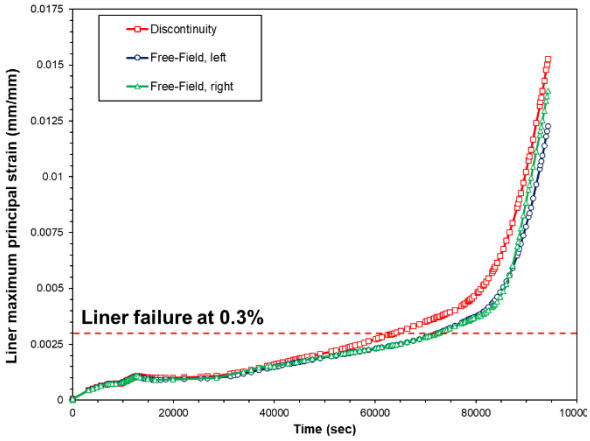

Fig. 8. Maximum principal strains of the liner at the EH and FFs [6]

4. Conclusion

This paper focused on evaluating the leak failure in the PWR containment building under combined temperature and internal pressure loads. The subsequent key points were emphasized.

(1) By conducting a mesh sensitivity study, the finite element model's accuracy and precision for the PWR containment building were verified.

(2) Heat transfer coefficients for convection and conduction were incorporated into a heat transfer analysis, which was then integrated into the structural analysis considering material property degradations due to temperature changes.

(3) The failure pressures were analyzed based on the ASME code criteria of 0.3% liner strain. Liner tears were expected to occur at 0.61 MPa at the EH, and at 0.67 MPa and 0.66 MPa near the left and right FF regions, respectively.

ACKNOWLEGMENT

This work was supported by the Nuclear Safety Research Program through the Korea Foundation Of Nuclear Safety (KoFONS) using the financial resource granted by the Nuclear Safety and Security Commission (NSSC) of the Republic of Korea (No. 2106008).

REFERENCES

[1] ASME Boiler and Pressure Vessel Code, Section III, “Rules for Construction of Nuclear Power Plant Components,” Division 2, American Society of Mechanical Engineers, New York, NY.

[2] ABAQUS-6.12. 2018. ABAQUS analysis user’s manual. ABAQUS 6.12, Dassault Systèmes Simulia Corp., Providence, RI, USA.

[3] Hognestad, E. 1951. A study on combined bending and axial load in reinforced concrete members. University of Illinois at Urbana-Champaign, IL, 43−46. Bulletin.

[4] Izumo, J., Shima, H., Okamura, H., 1989. Analytical model for RC panel elements subjected to in-plane forces. Concrete Library Japan Society of Civil Engineers. 12, 155–181.

[5] Cho, W.M., Ha, S.K., Kang, S.H.S., Chang, Y.S. 2023. A numerical approach for assessing internal pressure capacity at liner failure in the expanded free-field of the prestressed concrete containment vessel, Nuclear Engineering Technology 55, 3677-3691.

[6] Cho, W.M., Cho, Y.J., Ha, S.K. 2024. Probabilistic assessment of internal pressure capacity of OPR-1000 at leak under hydrogen burning conditions, In preparation.

[7] Jovall, O., Paalsson, M., Svaerd, B., Larsson, Jan-Anders. 2005. ISP 48: Posttest analysis of the NUPEC/NRC 1:4-scale prestressed concrete containment vessel model (NEA-CSNI-R-2005-05), Nuclear Energy Agency of the OECD (NEA).